Catal Lett (2017) 147:2134–2143
DOI 10.1007/s10562-017-2100-y

Facile pH-Dependent Synthesis and Characterization of Catechol Stabilized Silver Nanoparticles for Catalytic Reduction of 4-Nitrophenol

Hailemariam Gebru[1] · Saide Cui[1] · Zhenjiang Li[1] · Xin Wang[1] · Xianfu Pan[1] · Jingjing Liu[1] · Kai Guo[1]

Received: 30 March 2017 / Accepted: 28 May 2017 / Published online: 28 June 2017
© Springer Science+Business Media, LLC 2017

Abstract Catalysis by silver nanoparticles (Ag-NPs) in organic transformations has received growing attention due to their unique reactivity and selectivity. Herein, we investigated a versatile one-step approach for synthesizing thermally stable AgNPs using catechol (1,2-benzenediol) without additional reducing and stabilizing agents in aqueous solution. In an alkaline environment, oxidation of catechol played a dual role in the reduction of silver ions (Ag^+) and stabilization of the AgNPs. Nanoparticles with different size and morphology were obtained under different experimental conditions. X-ray diffraction (XRD) analysis suggests the formation of crystalline AgNPs of average size 13, 38 and 47 nm and face centered cubic structure as the reaction pH varied. As demonstrated in dynamic light scattering (DLS) and scanning electron microscopy (SEM) images, AgNPs with uniform size distribution (50 nm) were synthesized at pH 11. The nanoparticles are thermally stable with a steady loss of weight up to 800 °C as confirmed by thermogravimetric analysis (TGA). Comparing to AgNPs@pH5 and AgNPs@pH8, AgNPs synthesized at pH 11 have shown significant catalytic activity in the reduction of 4-nitrophenol (4-NP) to 4-aminophenol (4-AP) with 61% conversion at 20 °C. The results suggested that stable and monodisperse nanoparticles with tunable catalytic activity could be produced as the pH of the reaction was altered.

Electronic supplementary material The online version of this article (doi:10.1007/s10562-017-2100-y) contains supplementary material, which is available to authorized users.

✉ Zhenjiang Li
zjli@njtech.edu.cn

✉ Kai Guo
guok@njtech.edu.cn

[1] State Key Laboratory of Materials-Oriented Chemical Engineering, College of Biotechnology and Pharmaceutical Engineering, Nanjing Tech University, 30 Puzhu Rd South, Nanjing 211816, China

Graphical Abstract

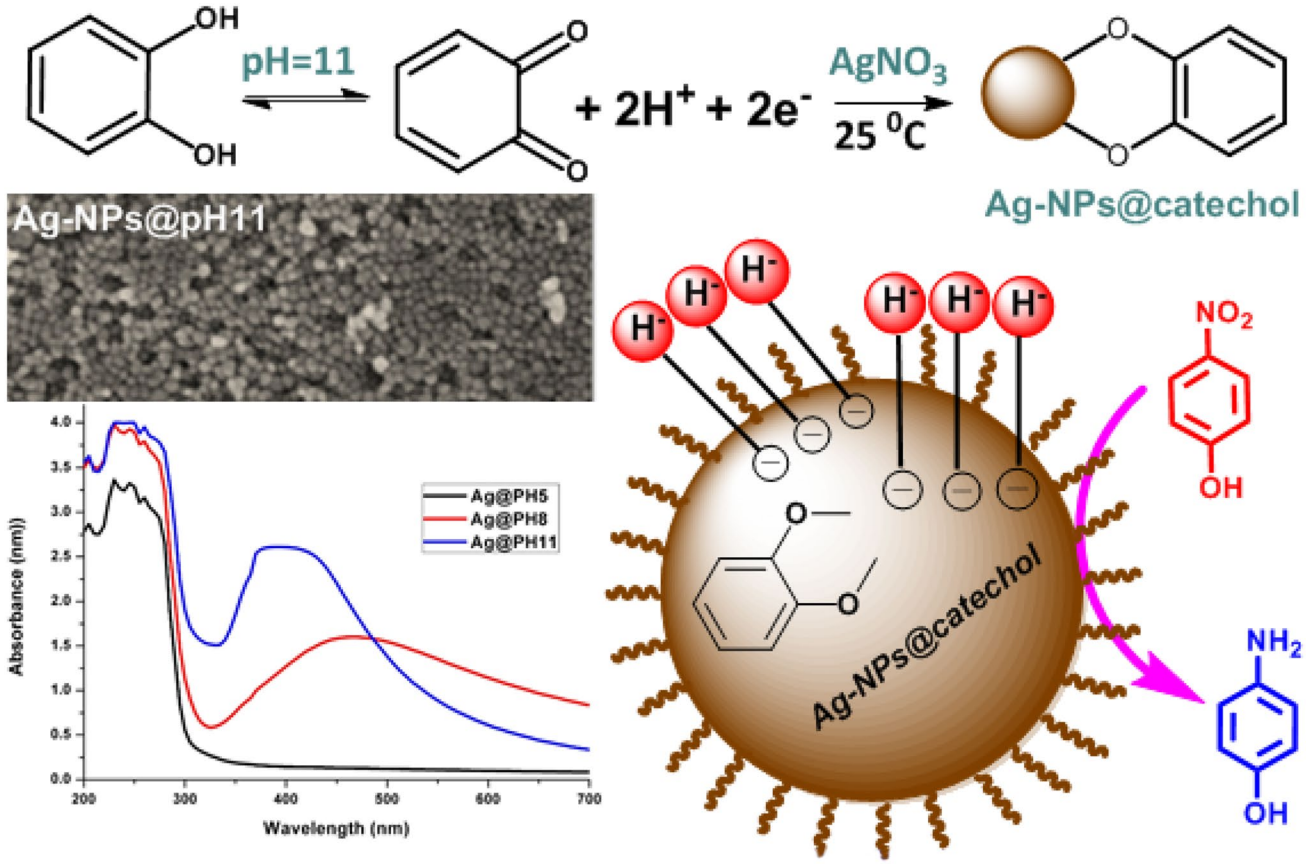

Keywords Silver nanoparticles · Catechol · Stabilization · Size-distribution · Reduction

1 Introduction

Noble metal nanoparticles have received much attention in catalysis [1–3] and medicine [4–6] owing to their unique optical and electronic properties. In particular, silver nanoparticles (AgNPs) have shown a remarkable catalytic activity, high reactivity and excellent selectivity [7, 8]. AgNPs catalyzed reduction of 4-nitrophenol (4-NP) to 4-aminophenol (4-AP) by borohydride ion have been widely investigated [9–13]. However, their susceptibility to aggregation could possibly diminish the surface area available for interaction, and limit their applicability [14]. To overcome this situation, AgNPs were fabricated using different capping agents such as cationic polyborons,[1] catechin,[15] fibrous nano-silca,[8] sugar based amphiphiles,[16] and composite copolymers [4]. Similarly, aggregation and morphology of the AgNPs were delicately tuned by pH, time and reaction temperature [17, 18].

Substantial work in the preparation of stable and monodispersed silver nanoparticles has been disclosed [5, 19, 20]. The synthesis of metal nanoparticles using raw plant extract is considered as a green alternative [21] to the traditional ones that empolyed harmful chemicals as reducing agents [22] and pose an environmental threat [23]. However, the nature of the capping molecules and exact surface properties of nanoparticles have remained unclear. It has been indicated that the biomolecules in raw plant extract are likely responsible for controlling the size of nanoparticle through surface activity [24] due to their indefinitive structures upon seasonal change. Likewise, the adsorption of organic molecules on the surface of the nanoparticles could block the available active sites which are required for metal catalyzed reactions [25]. Consequently, natural reducing and stabilizing agents with definitive chemical structure [26–30] have been used to synthesize monodisperse nanocrystals.

In this regard, a natural 1,2-benzenediol, catechol, which has been widely explored for the exceptional binding affinity and reducing power,[31–35] attracted our interest. For instance, Lee and co-worker denoted the use of polyphenol derivatives with additional functional groups can produce different Au nanostructures [23]. In another example, Roy et al. discussed the simultaneous reduction of Au^{3+} ions and growth of AuNPs on polydopamine [36]. However, the

effect of reaction parameters on the formation and stabilization of AgNPs associated to catechol oxidation requires further investigation. Accordingly, we hypothesized that biomolecules with definitive chemical structure could simultaneously reduce metal ions and stabilize metal nanoparticles to control the size and tune the catalytic activity as the reaction pH altered. To support our assumption, we attempted to prepare stable and monodisperse silver nanoparticles by catechol as reducing and stabilizing agent for effective catalysis in the reduction of 4-NP. We chose catechol since it is easily accessible, inexpensive and natural reducing and stabilizing agent. Moreover, the synthesis approach employed here is not only facile, cost-effective and green but also provides an insight toward the synthesis of metal nanoparticles by biomolecules with known chemical structure in an eco-friendly aqueous solvent.

In this work, we investigated the synthesis of AgNPs by catechol without additional reducing and stabilizing agents at different reaction conditions. Three samples of silver nanoparticles, i.e. Ag@pH5, Ag@pH8, and Ag@pH11 were prepared by mixing aqueous solutions of catechol and silver nitrate and adjusting the reaction pH at 5, 8, and 11. Herein, we report (1) the use of catechol as both reducing and stabilizing agent for the synthesis of AgNPs in aqueous solution, (2) the effect of the amount of reducing agent, solution pH and reaction time on the formation of AgNPs, (3) characterizations of AgNPs by UV–Vis spectroscopy, XRD, DLS, SEM, TGA and DSC, (4) AgNPs catalyzed reduction of 4-NP to 4-AP in the presence of sodium borohydride as a reducing agent.

2 Experimental Section

2.1 Materials

Silver nitrate ($AgNO_3$, 99.8%), catechol ($C_6H_6O_2$, 98%), sodium hydroxide (NaOH; 96%), sodium borohydride ($NaBH_4$, 98%), 4-nitrophenol (4-NP, 98%) were purchased from Sinopharm Chemical Reagent Co, Ltd, and used as received. Distilled water was used as a solvent for the preparation of all solutions.

2.2 Synthesis of Silver Nanoparticles

The pH of an aqueous solution of catechol was adjusted to 8 and 11 by adding 1 M NaOH drop by drop. The basic solution of 4 mL of 10^{-2} M catechol was added dropwise to the aqueous solution of 10 mL of 10^{-2} M $AgNO_3$ in 50 mL Erlenmeyer flask at room temperature. The progress of the reaction was monitored via UV–Vis spectrophotometer. The sample solutions were prepared by taking 100 µL from the suspension and diluted in 900 µL distilled water. Then, 200 µL of the diluted form of the suspension was used for measurement. The absorbance was measured in triplicate. The product was washed and centrifuged three times at 6000 rpm for 10 min. The supernatant was removed and the precipitate was dried in an oven and kept for further characterization.

2.3 Optimization of Reaction Parameters

To evaluate the effect of the amount of reducing agent, 1–4 mL of catechol solution was added to 10 mL of 10^{-2} M $AgNO_3$. Then, different volumes of 0.1 M NaOH was added to the optimum ratio of the reducing agent and $AgNO_3$. The kinetic reduction of Ag^+ ions to AgNPs was monitored by absorbance measurements. Moreover, three different samples of AgNPs named Ag@pH5, Ag@pH8 and Ag@pH11 were synthesized by adjusting 10^{-2} M catechol solution by 1 M NaOH and mixing with aqueous solution of $AgNO_3$.

2.4 Characterization

Absorbance measurement was done on Molecular devices spectra Max M3 spectrophotometer. The size distribution of the nanoparticles was analyzed by Dynamic Light Scattering (DLS) Malvern Instruments Zetasizer Nano S90 with a He-Ne laser (633 nm, 4 mW) at room temperature. Sample solutions were prepared in distilled water having a concentration of 10 mg mL^{-1}. SEM measurements were performed using Hitachi S-4800 scanning electron microscope. Thermogravimetric analysis (TGA) and differential scanning calorimetry (DSC) were carried out on a TGA NETZSCH STA 449F3 instrument at a heating rate of 10 °C min^{-1} from room temperature up to 800 °C under a nitrogen atmosphere (50 cm^3 min^{-1}). X-ray diffraction (XRD) patterns were recorded in the reflection mode under Cu K α radiation ($\lambda = 0.1542$ nm) and operating at 40 kV and 40 mW by using a Bruker-AXS D8 ADVANCE X-ray diffractometer (Germany). Origin version 8 and XRD High Score soft wares were used for spectral analysis obtained from the spectroscopic instruments.

2.5 Catalytic Conversion

The reduction of 4-NP to 4-AP as a benchmark reaction was employed to evaluate the catalytic activity of the as-prepared AgNPs. Initially, 100 µL of 0.1 M $NaBH_4$ was added to a test tube containing 1.25 mL of 1 mM 4-NP solution [37]. Then, 200 µL of AgNPs suspension in distilled water was added to the mixture of 4-NP and $NaBH_4$. For absorbance measurement, 100 µL of the mixture was taken and diluted with 900 µL distilled water. The reaction was monitored through periodic sampling from 0 to 60 min on UV–Vis spectrophotometer for spectral and kinetic

measurement. The percentage catalytic conversion of 4-NP was calculated by the equation below from the absorbance readings taken at the initial time (A_0) and time t (A_t) at 60 min.

$$\% \text{ Conversion} = \frac{A_0 - A_t}{A_0} \times 100 \quad (1)$$

where A_t is the absorbance of 4-NP measured at time t; A_0 is the absorbance of 4-NP measured at time zero [14].

3 Results and Discussion

3.1 Preparation of AgNPs

Catechol was used as reducing and stabilizing agent to prepare AgNPs at room temperature. When an aqueous solution of $AgNO_3$ was added to catechol solution under alkaline environment, rapid change in color was observed within 20 min. The formation of AgNPs was confirmed by the rapid change in color at higher pH of the reaction mixture (Fig. S1). This is due to oxidation of two vicinal hydroxyl groups in catechol to quinones providing two electrons at basic condition [38, 39] which are responsible for simultaneous reduction of Ag^+ ions and stabilization of AgNPs. Their ability to coordinate strongly to metal surface through two adjacent hydroxyls, covalently cross-linked and releasing electrons when oxidized to quinones [40] provides further stability of the AgNPs.

3.2 UV–visible Spectroscopy

The characteristic surface plasmon resonance (SPR) peaks at $\lambda_{max} = 395$ and 400 nm was observed due to the formation of AgNPs[16]. The SPR is related to the size, and the gradual increase in absorbance is due to an increase in the size of AgNPs. Initially, AgNPs were prepared by adding 1–9 mL of 10^{-2} M catechol solution to a flask containing 10 mL of 10^{-2} M $AgNO_3$ solution. As demonstrated in Fig. S2, at a lower amount of reducing agent (1 mL) no SPR peak observed, but with increasing the amount of the reducing agent in a basic medium, a significant increase in absorbance peak was observed, which confirmed the formation of AgNPs.

3.3 Optimization of Reaction Parameters

The preparation of AgNPs was carried out at different reaction parameters such as amount of reducing agent, reaction pH, time, and the nature of the stabilizing agent [17, 18, 41]. The characteristic absorbance peak of AgNPs implied that catechol solution at different reaction condition acts as both reducing and stabilizing agent due to its oxidative self-condensation nature [33].

3.4 Amount of Reducing Agent

In order to identify the optimum amount of catechol and the concentration of $AgNO_3$, we carried out a series of experiments. Based on our screening, 4:10 (V/V) ratio of reducing agent to $AgNO_3$ gave an optimal absorbance, and this proportion was used throughout the experiment. As the amount of reducing agent increased, a gradual increase in absorbance observed. This indicates the formation of AgNPs with increasing the amount of catechol (Fig. 1a) [42].

3.5 Reaction pH

As the amount of NaOH increases, an increase in absorbance intensity of AgNPs was observed (Fig. 1b). A solution with dark brown color was observed at pH 11 with enhanced SPR band near 400 nm. This showed that the oxidation and redox potential of catechol are dependent on the volume of NaOH. Previous studies suggested that the pH dependence of the catechol redox process can be ascribed to a two proton–two electron ($2H^+2e^-$) transfer, called a proton-coupled electron transfer reaction [39, 40, 43]. Hence, catechol played a dual role as reducing and stabilizing agent in the synthesis of AgNPs.

3.6 Kinetics of Ag^+ Ions Reduction

Upon the addition of basic solution of catechol to aqueous solution of $AgNO_3$, rapid change in color was observed as soon as the two solutions mixed. This indicates the reduction of Ag^+ ions to AgNPs at pH 11 took place within short time frame. The slight increase in absorbance at $\lambda_{max} = 400$ from the initial time to 20 min reaction is due to the fast reduction of Ag^+ ions and formation of the nanoparticles (Fig. 1c, d).

3.7 Dynamic Light Scattering (DLS) Analysis

To investigate the size distribution of AgNPs the test solutions were prepared in distilled water. Fig. S3 demonstrates the formation of AgNPs with uniform size distribution. The hydrodynamic diameter was found to be 121, 131 and 174 nm for the samples Ag@pH11, Ag@pH8 and Ag@pH5 respectively. The particle diameter measured using DLS is bigger as compared to that of XRD and SEM due to the adsorption of substances associated to catechol self-condensation on the surface of the nanoparticles and solvation shell moving along with the particle [44] besides the size of the core particle (Fig. S3). At lower concentration of

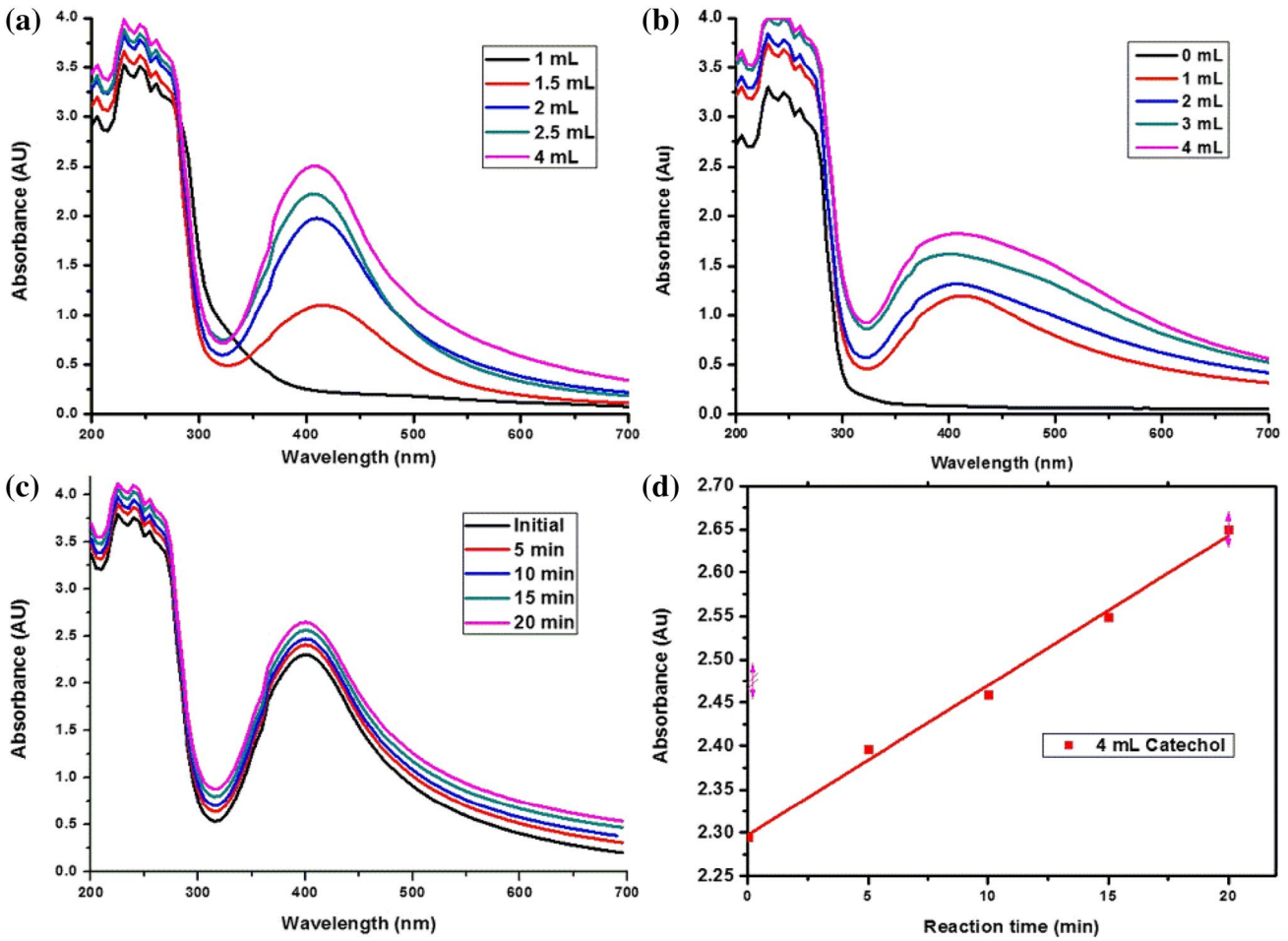

Fig. 1 UV–Vis spectra of catechol capped silver nanoparticles. **a** 10 mL of 10^{-2} M $AgNO_3$ and 1–4 mL of 10^{-2} M catechol **b** effect of addition of 0.1 M NaOH to 4 mL of catechol and 10 mL of $AgNO_3$, **c** reaction time at pH 11 and **d** absorbance time graph

the metal salt ($AgNO_3$), nanoparticles with small and uniform size distribution could be achieved [16].

3.8 X-ray Diffraction Study

The XRD patterns of three different samples of AgNPs are displayed in Fig. 2. Accordingly, the expected Bragg diffraction angles of Ag-NPs at 38.12°, 44.34°, 64.40°, 77.33°, 81.40° in the XRD pattern correspond to (111), (200), (220), (311), and (222) planes of face-centered cubic (FCC) crystal structure of crystalline Ag-NPs [8, 45]. The average crystallite size of Ag-NPs calculated on the basis of reflection width by Debye–Scherrer equation;

$$\tau = \frac{\kappa\lambda}{\beta cos\theta} \quad (2)$$

where τ is average crystallite domain size; κ is dimensionless shape factor with value close to unity (0.94); λ is X-ray wavelength;β is the line broadening at half maximum intensity XRD spectrum; θ is diffraction angle;

The average crystallite size of the three samples named Ag@pH = 5, Ag@pH = 8, and Ag@pH = 11 was found to be 47, 38 and 13 nm respectively [46]. As calculated by Eq. 2 the average crystallite size of the sample prepared at pH 11 is very small comparing to AgNPs prepared at pH 5 and 8. This indicates that catechol redox potential and oxidative self-condensation are highly dependent on the pH of the reaction mixture which in turn influence the size of the particles. As a result, crystallographic nature and the number of active sites is related to catalytic activity of AgNPs [47].

3.9 Scanning Electron Microscopy (SEM)

The shape and size of catechol stabilized silver nanoparticles of the three samples named, Ag@pH5, Ag@pH8 and Ag@pH11 determined by this technique. As shown in Fig. 3c, spherical nanoparticles with a uniform size distribution of 50 nm were obtained at pH 11. The result suggests a close agreement to the nanoparticles synthesized

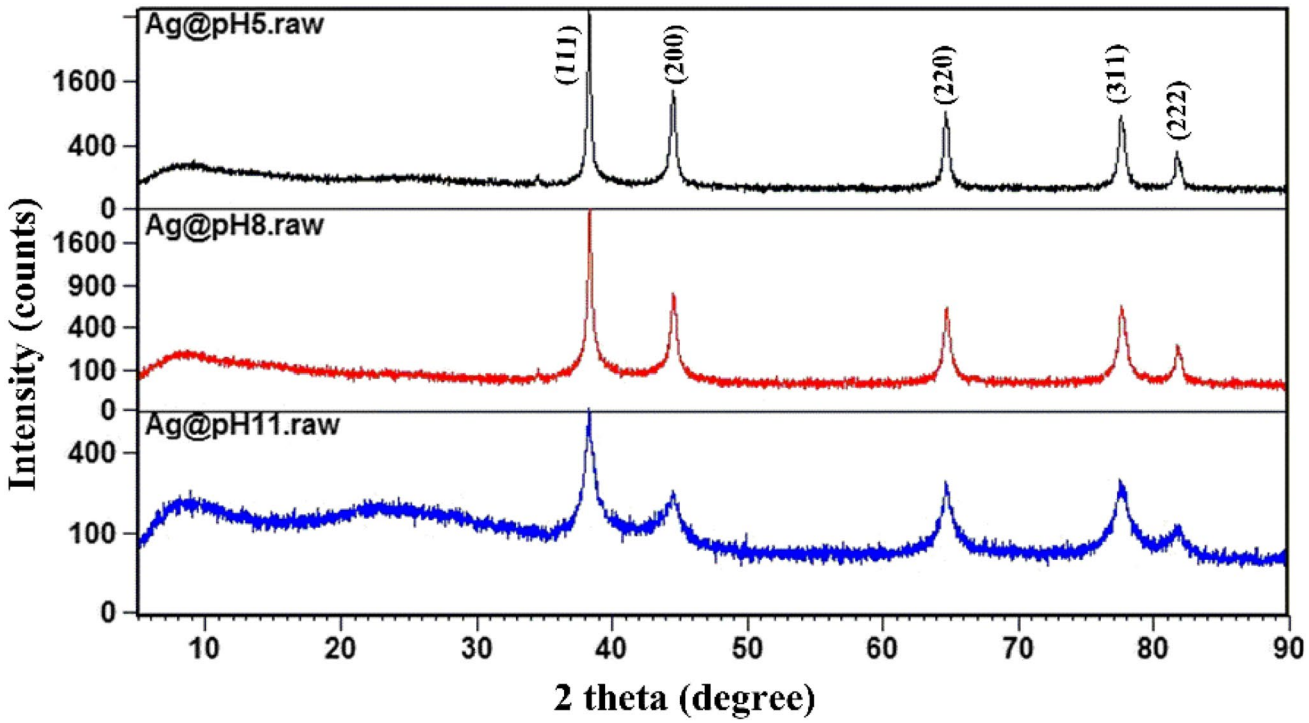

Fig. 2 XRD pattern of catechol stabilized silver nanoparticles at three different pH values; Ag@pH5 (*Red*), Ag@pH8 (*Blue*), and Ag@pH11 (*Green*)

using additional reducing and protecting agents.[23, 32] In addition, Ag@pH11 has shown a relatively better intensity or absorption peak (Fig. 3d, Blue) comparing to the Ag@pH5 and Ag@pH8 (Fig. 3a, b). The absence of SPR peak for Ag@pH5 in the Uv–visible spectrum (Black) as the reduction of Ag^+ ions is less pronounced. As compared to Ag@pH5, sample Ag@pH8 of AgNPs shows a better distribution of particles and the formation of the nanoparticles was observed in SEM image and Uv–Vis spectra (Red). As reaction mixture gets more basic, the formation of stable and uniformly distributed nanoparticles is due to the dependence of catechol oxidation and redox activity on pH [48].

3.10 Thermal Analysis of AgNPs

The thermal stability of the obtained AgNPs was analyzed by TGA. The nanoparticles synthesized by this approach are thermally stable up to 800 °C with weight loss less than 11%. The weight losses of Ag@pH11, Ag@pH5, and Ag@pH8 were found to be 11, 8 and 1% respectively [49]. TGA and DSC spectra imply the formation of thermally stable AgNPs and the decomposition of the adsorbed substances associated with catechol oxidation and self-condensation on the surface of nanoparticles after 300 °C with less than 11% weight loss (Fig. 4a, b).

3.11 Catalytic Conversion

AgNPs are the most widely used catalysts in the transformation of fine chemicals to enhance the rate of degradation [1, 50]. We have chosen the reduction of 4-nitrophenol to 4-aminophenol as a model reaction in order to examine the catalytic activity of AgNPs. The reduction of 4-NP to 4-AP was monitored by absorbance reading at a maximum wavelength of 400 nm. Silver nano-catalyst enhanced the rate of degradation of 4NP in the presence of reducing agent ($NaBH_4$). Upon addition of AgNPs to a reaction mixture containing 4-NP and NaOH with the interval of 0–60 min reaction time, the conversion of 4-NP to 4-AP reached 61%, 33% and 17% for samples Ag@pH11, Ag@pH8 and Ag@pH5 respectively (Table S1). The catalytic conversion of 4-NP is associated with the size of the nanoparticles. The concentration of AgNPs has a significance influence in the reduction of 4NP and completion [16, 51]. After the addition of $NaBH_4$ to 4NP solution, the disappearance of 4NP confirmed by its characteristic absorption maximum at 317 nm in water with a shift to 400 nm due to the formation of the p-nitrophenolate ion [1]. Moreover, with a prolonged reaction time, increasing temperature and varying the [4-NP]/[AgNPs] ratio 100% conversion could be achieved (Fig. S4). The size of the particles played a key role in the catalytic conversion of 4-NP to 4-AP which is related to the surface area available for interaction at the surface.

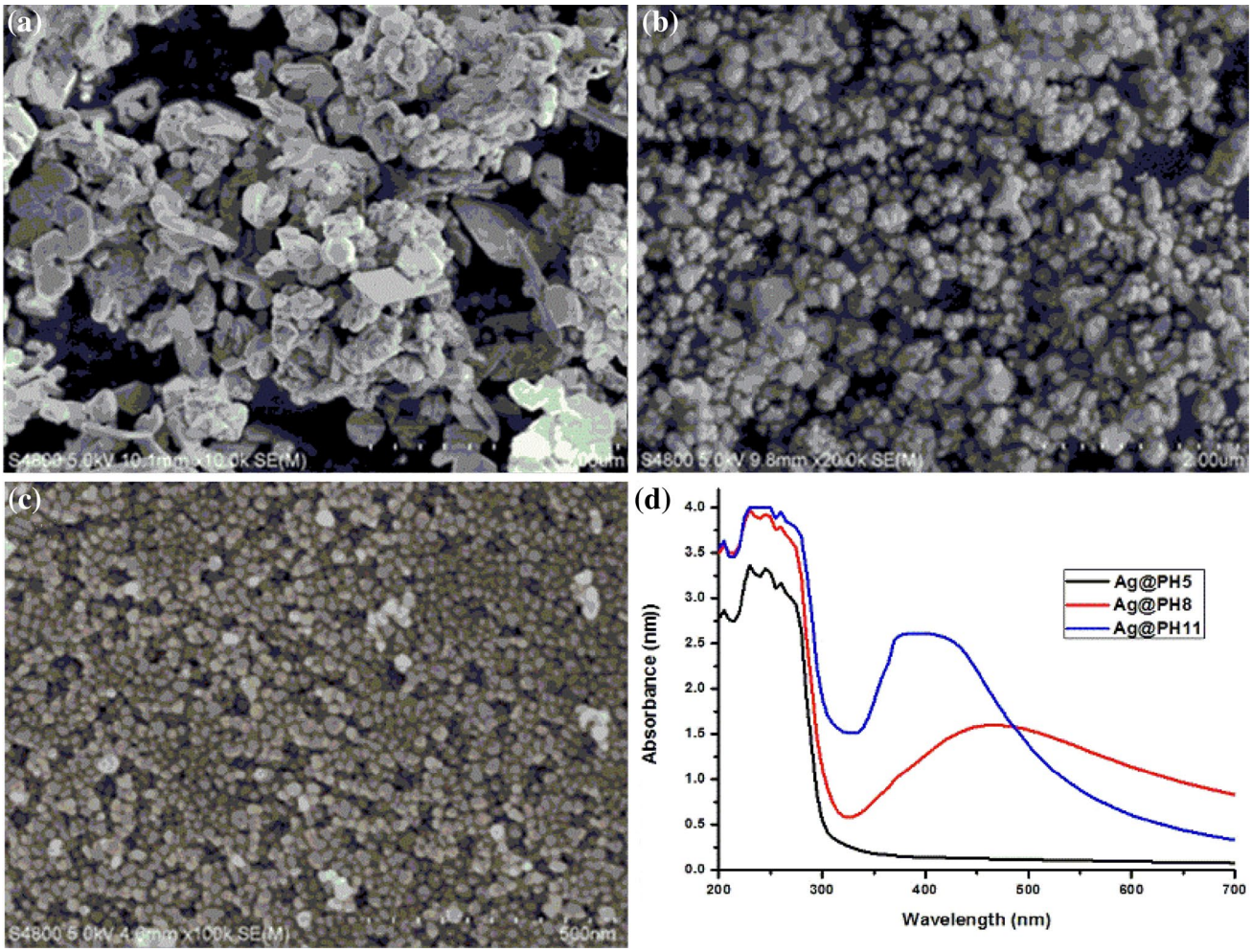

Fig. 3 SEM images of silver nanoparticles synthesized at **a** pH 5, **b** pH 8, **c** pH 11 and **d** Uv–visible spectra of three samples of silver nanoparticles; Ag@pH5 (*Black*), Ag@pH8 (*Red*) and Ag@pH11 (*Blue*)

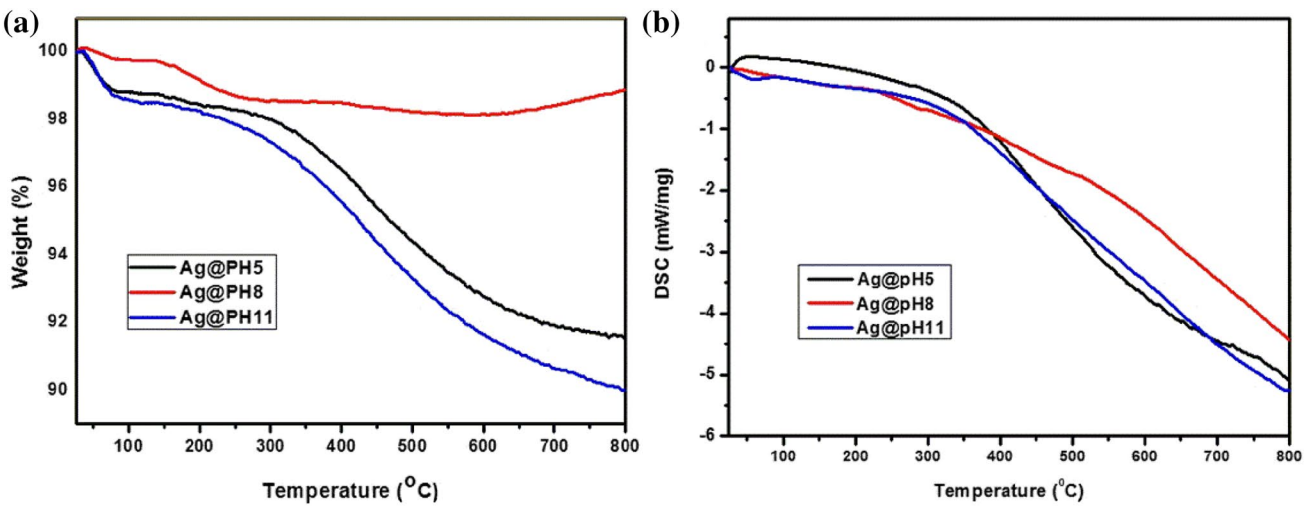

Fig. 4 Thermogravimetric analysis (*left*) and DSC spectra (*right*) of catechol stabilized silver nanoparticles; Ag@pH5 (*black*), Ag@pH8 (*red*) and Ag@pH11 (*blue*)

In this typical reaction, after addition of AgNPs to the mixture of 4NP and $NaBH_4$ the color gradually faded with time which implied the reduction of 4-NP to 4-AP (Fig. 5a). The catalytic decomposition of 4-AP by $NaBH_4$ confirmed by the gradual decrease in the intensity of the absorbance peak with time at 400 nm (Fig. 5b) [52, 53]. Since the concentration of $NaBH_4$ as compared to 4-NP is very high and the reaction is expected to be independent of the amount of borohydride. Accordingly, the kinetic data for the reduction of 4-NP can be fitted to a Langmuir–Hinshelwood apparent first-order plot [14, 54].

$$Rate(r) = -\frac{dC}{dt} = \frac{\kappa KC}{(1 + KC)} \tag{3}$$

where r can be defined as the rate of disappearance of 4-NP, C is the concentration of the reactant, t is the reaction time, κ represents the reaction rate constant; K is adsorption coefficient of the reactant. Assuming the initial concentration is very small the rate can be expressed as apparent first order [49];

$$r = -\frac{dC}{dt} = \kappa KC \tag{4}$$

$$-\ln\left(\frac{C_t}{C_0}\right) = \kappa KC = K_{app}t \tag{5}$$

K_{app} is the apparent first-order rate constant (s^{-1}). The rate of conversion of the reactant is monitored by Uv–Vis spectrometer from absorbance measurements since the ratio of the concentration of 4-NP (C_t) at time t to its initial concentration C_0 at t=0 is directly given by the ratio of respective absorbance $[A]_t/[A]_0$. According to the apparent first-order rate equation, ln (A_t /A_0) is proportional to time, the reaction rate corresponds to the slope k_{app} of the curve.

$$-\ln\left(\frac{C_t}{C_0}\right) = -\ln\left(\frac{A_t}{A_0}\right) = K_{app}\, t \tag{6}$$

$$\ln\left(\frac{A_t}{A_0}\right) = -K_{app}\, t \tag{7}$$

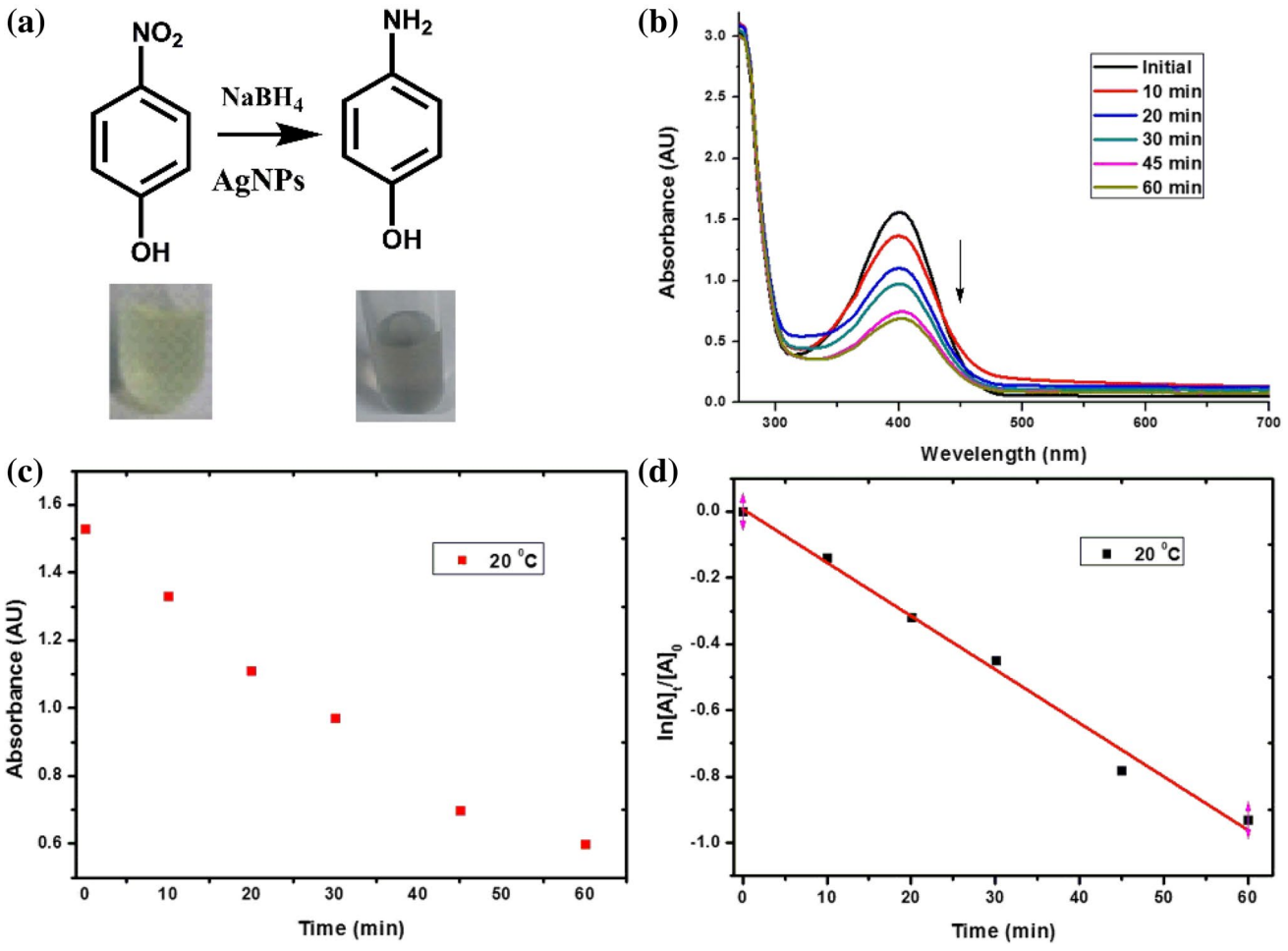

Fig. 5 Nano-silver catalyzed reduction of 4-nitrophenol in the presence of $NaBH_4$ **a** conversion of 4-NP to 4-AP, **b** its gradual decrese in absorbance, **c** absorbance versus time graph, **d** kinetic plot

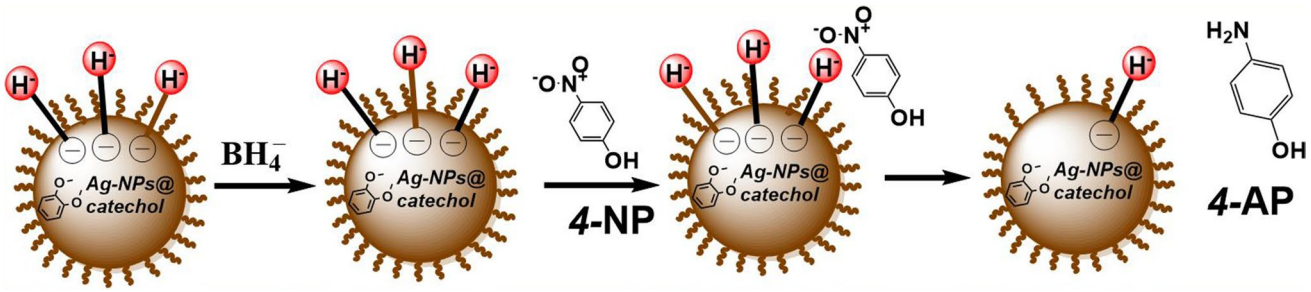

Fig. 6 Schematic representation of mechanism of nano-silver catalyzed reduction of 4-nitrophenol (4-NP) to 4-aminophenol (4-AP) in the presence of sodium borohydride as a reducing agent

Reaction rate expressed in terms of the rate of decomposition of 4-NP. The absorbance versus time graph indicates the catalytic reaction followed first order kinetics (Fig. 5c, d). The rate constant was determined from the plot of ln([A]t/[A]0) versus time graph and its value is 1.6×10−2 min−1. The results obtained imply that AgNPs@catechol catalyzed reduction of 4-NP is in agreement with literature reports [9, 49, 55].

The mechanism of catalytic reduction takes place on the surface Ag nanoparticles [49]. The extent of the catalytic reaction depends on the surface area available for interaction. The smaller the particle the greater is its surface area to volume ratio. Their crystallographic nature plays a key role for reactions which occur on the surface. The adsorption of 4-NP onto the particle surface contributes to hinder the kinetic barrier of the reaction [46, 47, 56].

The catalytic reduction proceeds on the surface of the metal nanoparticles in such a way that BH_4^- ions react with the surface of the nanoparticle to form a surface-hydrogen species and 4-NP adsorbs onto unoccupied sites. Due to fast adsorption/desorption process of both reagents on the surface, the reaction is modelled in terms of a Langmuir isotherm (Fig. 6) [54].

4 Conclusion

A versatile, economically viable and pH-dependent approach was established to prepare stable silver nanoparticles with relatively uniform size distribution. This method of nanoparticle synthesis is a green chemistry approach since catechol, which found in mussel foot proteins, was used as reducing and stabilizing agent and water as a solvent. Likewise, we have emphasized on the formation of AgNPs at different reaction parameters including the amount of reducing agent, pH and reaction time. As a result, the amount of reducing agent significantly influences the size and formation of AgNPs. Thermally stable NPs with less than 11% weight loss and uniform size distribution were synthesized. The stability of the nanoparticles is due to oxidation self-condensation of catechol at the alkaline environment. The results suggested that catechol plays a dual role in the reduction of Ag^+ ions and stabilization of AgNPs. Furthermore, AgNPs which are synthesized at pH 11 demonstrated higher catalytic performance in the reduction of 4-NP to 4-AP with a conversion of 61% at 20 °C. The as-synthesized Ag-NPs may be used as a promising catalyst in the degradation of organic pollutants.

Acknowledgements The National Natural Science Foundation of China (U1463201, 21522604), Natural Science Foundation of Jiangsu Province, China (BK20150031), Jiangsu National Synergetic Innovation Center for Advanced Materials (SICAM), and the Priority Academic Program Development of Jiangsu Higher Education Institutions (PAPD) are gratefully ackowleged for funding this work. We would like to thank Prof. He Huang (Nanjing Tech University) for providing access to UV–Vis spectrophotometer.

References

1. Baruah B, Gabriel GJ, Akbashev MJ, Booher ME (2013) Langmuir 29:4225–4234
2. Takale BS, Bao M, Yamamoto Y (2014) Org Biomol Chem 12:2005–2027
3. Zhang Y, Diao W, Monnier JR, Williams CT (2015) Catal Sci Technol 5:4123–4132
4. Lu Z, Zhang X, Li Z, Wu Z, Song J, Li C (2015) Polym Chem 6:772–779
5. Sharma VK, Yngard RA, Lin Y (2009) Adv Colloid Interface Sci 145:83–96
6. Dallas P, Sharma VK, Zboril R (2011) Adv Colloid Interface Sci 166:119–135
7. Nigra MM, Ha J-M, Katz A (2013) Catal Sci Technol 3:2976–2983
8. Dong Z, Le X, Li X, Zhang W, Dong C, Ma J (2014) Appl Catal B 158:129–135
9. Ciganda R, Li N, Deraedt C, Gatard S, Zhao P, Salmon L, Hernandez R, Ruiz J, Astruc D (2014) ChemCommun 50:10126–10129
10. Holden MS, Nick KE, Hall M, Milligan JR, Chen Q, Perry CC (2014) RSC Adv 4:52279–52288
11. Shin KS, Choi J-Y, Park CS, Jang HJ, Kim K (2009) Catal Lett 133:1–7
12. Vadakkekara R, Chakraborty M, Parikh PA (2014) Colloid J 76:12–18

13. Sharma M, Sarma PJ, Goswami MJ, Bania KK (2017) J Colloid Interface Sci 490:529–541
14. Geng Q, Du J (2014) RSC Adv 4:16425–16428
15. Choi Y, Choi M-J, Cha S-H, Kim YS, Cho S and Park Y (2014) Nanoscale Res Lett 9:1–8
16. Eising R, Elias WC, Albuquerque BL, Fort S, Domingos JB (2014) Langmuir 30:6011–6020
17. Sun YG, Xia YN (2002) SCIENCE 298:2176–2179
18. Zhang Q, Xie J, Yu Y, Lee JY (2010) Nanoscale 2:1962–1975
19. Moulton MC, Braydich-Stolle LK, Nadagouda MN, Kunzelman S, Hussain SM, Varma RS (2010) Nanoscale 2:763–770
20. Kouvaris P, Delimitis A, Zaspalis V, Papadopoulos D, Tsipas SA, Michailidis N (2012) Mater Lett 76:18–20
21. Hebbalalu D, Lalley J, Nadagouda MN, Varma RS (2013) ACS Sustainable Chem Eng 1:703–712
22. Navaladian S, Viswanathan B, Viswanath RP, Varadarajan TK (2007) Nanoscale Res Lett 2:44–48
23. Lee Y, Park TG (2011) Langmuir 27:2965–2971
24. Adil SF, Assal ME, Khan M, Al-Warthan A, Siddiqui MRH, Liz-Marzan LM (2015) Dalton Trans, 44:9709–9717
25. Metz KM, Sanders SE, Pender JP, Dix MR, Hinds DT, Quinn SJ, Ward AD, Duffy P, Cullen RJ, Colavita PE (2015) ACS Sustainable Chem Eng, 3:1610–1617
26. Liu J, Qin G, Raveendran P, Ikushima Y (2006) Chem Euro J, 12:2131–2138
27. Huang HZ, Yang XR (2004) Biomacromolecules 5:2340–2346
28. Vigneshwaran N, Nachane RP, Balasubramanya RH, Varadarajan PV (2006) Carbohydr Res 341:2012–2018
29. Murugadoss A, Kai N, Sakurai H (2012) Nanoscale 4:1280–1282
30. Kalwar NH, Nafady A, Soomro RA, Sirajuddin, Sherazi STH, Khaskheli AR, Hallam KR (2015) Rare Met 34:683–691
31. Ma Y-r, Niu H-y, Zhang X-l and Cai Y-q (2011) Chem Commun 47:12643–12645
32. Marcelo G, Fernandez-Garcia M (2014) RSC Adv 4:11740–11749
33. Wu J, Zhang L, Wang Y, Long Y, Gao H, Zhang X, Zhao N, Cai Y, Xu J (2011) Langmuir 27:13684–13691
34. Black KCL, Liu Z, Messersmith PB (2011) Chem Mater 23:1130–1135
35. Sedo J, Saiz-Poseu J, Busque F, Ruiz-Molina D (2013) Adv Mater 25:653–701
36. Roy AK, Park SY and In I(2015) Nanotechnology 26:105601
37. Li M, Chen G (2013) Nanoscale 5:11919–11927
38. Marcelo G, Lopez-Gonzalez M, Mendicuti F, Pilar Tarazona M and Valiente M (2014) Macromolecules 47:6028–6036
39. Xu H, Nishida J, Ma W, Wu H, Kobayashi M, Otsuka H, Takahara A (2012) ACS Macro Lett 1:457–460
40. Lin Q, Li Q, Batchelor-McAuley C, Compton RG (2015) J Phys Chem C 119:1489–1495
41. Soni SS, Vekariya RL, Aswal VK (2013) RSC Adv 3:8398–8406
42. Bleach R, Karagoz B, Prakash SM, Davis TP, Boyer C (2014) ACS Macro Lett 3:591–596
43. Fullenkamp DE, Barrett DG, Miller DR, Kurutz JW, Messersmith PB (2014) RSC Adv 4:25127–25134
44. Tomaszewska E, Soliwoda K, Kadziola K, Tkacz-Szczesna B, Celichowski G, Cichomski M, Szmaja W, Grobelny J (2013) J Nanomater. doi:10.1155/2013/313081.
45. Celen B, Ekiz D, Piskin E, Demirel G (2011) J Mol Catal A 350:97–102
46. Pandey S, Mishra SB (2014) Carbohydr Polym 113:525–531
47. Liang M, Su R, Huang R, Qi W, Yu Y, Wang L, He Z (2014) ACS Appl Mater Interfaces 6:4638–4649
48. Cong Y, Xia T, Zou M, Li Z, Peng B, Guo D, Deng Z (2014) J Mater Chem B 2:3450–3461
49. Tang J, Shi Z, Berry RM, Tam KC (2015) Ind Eng Chem Res 54:3299–3308
50. Dong X-Y, Gao Z-W, Yang K-F, Zhang W-Q, Xu L-W (2015) Catal Sci Technol 5:2554–2574
51. Kaestner C, Thuenemann AF (2016) Langmuir 32:7383–7391
52. Santos Kdo, Elias WC, Signori AM, Giacomelli FC, Yang H, Domingos JB (2012) J Phys Chem C 116:4594–4604
53. Mata R, Nakkala JR, Sadras SR (2015) Mater Sci Eng C 51:216–225
54. Wunder S, Lu Y, Albrecht M, Ballauff M (2011) ACS Catal 1:908–916
55. Ahmad A, Wei Y, Syed F, Imran M, Khan ZU, Tahir K, Khan AU, Raza M, Khan Q, Yuan QP (2015) RSC Adv 5:99364–99377
56. Gangula A, Podila R, Ramakrishna M, Karanam L, Janardhana C, Rao AM (2011) Langmuir 27:15268–15274